



This open access document is posted as a preprint in the Beilstein Archives at <https://doi.org/10.3762/bxiv.2022.63.v1> and is considered to be an early communication for feedback before peer review. Before citing this document, please check if a final, peer-reviewed version has been published.

This document is not formatted, has not undergone copyediting or typesetting, and may contain errors, unsubstantiated scientific claims or preliminary data.

Preprint Title Size and Frequency Dependent Heating Rates of Gold Nanoparticles Exposed to Radiofrequency Electric Field

Authors Justin Case, Kelly McNear, Mazen Alrahili, Viktoriia Savchuk, Andrii M. Lopatynskyi, Volodymyr Chegel and Anatoliy O. Pinchuk

Publication Date 18 Jul 2022

Article Type Full Research Paper

Supporting Information File 1 Supporting Information.docx; 5.2 MB

ORCID® IDs Andrii M. Lopatynskyi - <https://orcid.org/0000-0002-6847-892X>;
Anatoliy O. Pinchuk - <https://orcid.org/0000-0003-1721-5668>

License and Terms: This document is copyright 2022 the Author(s); licensee Beilstein-Institut.

This is an open access work under the terms of the Creative Commons Attribution License (<https://creativecommons.org/licenses/by/4.0>). Please note that the reuse, redistribution and reproduction in particular requires that the author(s) and source are credited and that individual graphics may be subject to special legal provisions.

The license is subject to the Beilstein Archives terms and conditions: <https://www.beilstein-archives.org/xiv/terms>.

The definitive version of this work can be found at <https://doi.org/10.3762/bxiv.2022.63.v1>

Size and Frequency Dependent Heating Rates of Gold Nanoparticles Exposed to Radiofrequency Electric Field

Justin Case,^{1,2} Kelly McNear,² Mazen Alrahili,³ Viktoriia Savchuk,^{1,2} Andrii M. Lopatynskyi,⁴ Volodymyr Chegel,⁴ and Anatoliy O. Pinchuk^{1,2}

¹ Department of Physics and Energy Science, University of Colorado Colorado Springs, 1420 Austin Bluffs Parkway, Colorado Springs, Colorado 80918, USA

² UCCS BioFrontiers Center, University of Colorado Colorado Springs, 1420 Austin Bluffs Parkway, Colorado Springs, Colorado 80918, USA

³ Physics Department, School of Science, Taibah University, Janadah Bin Umayyah Road, Medina 42353, Saudi Arabia

⁴ V.E. Lashkaryov Institute of Semiconductor Physics, National Academy of Sciences of Ukraine, 41, prospect Nauky, 03028 Kyiv, Ukraine

Abstract

Gold nanoparticles can be used as efficient nanotransducers of radiofrequency (RF) electromagnetic energy into heat, rendering them as excellent candidates for noninvasive hyperthermia treatment of cancer with minimal side effects. Here we report on experimental heating profiles of gold nanoparticles of various sizes (5 nm, 10 nm, 20 nm, and 30 nm) exposed to a capacitively coupled RF field at various frequencies (6.5 MHz, 8.2 MHz, 10 MHz, 13.56 MHz, 15 MHz, and 17 MHz). We find that the heating rates depend on the size of the gold nanoparticles and the frequency of RF irradiation. We use the energy balance equations to numerically simulate the heating profiles of the gold colloidal solutions.

Keywords

Gold nanoparticles, hyperthermia, RF E-field

Introduction

Cancer remains the number one cause of mortality around the globe and it is the major roadblock to increasing lifespan in developed countries.¹ Traditional cancer therapies such as surgery resection, radiation and chemotherapy are invasive and lead to severe side effects.² Moreover, prolonged

chemotherapy may lead to drug resistance and decrease its efficiency.² Novel nanotechnology enhanced methods to treat cancer are desirable to improve the efficiency of currently available cancer treatments.¹

Photothermal ablation of cancer cells has proven to be an effective treatment of cancer with minimal side effects.³ Gold nanoparticles of different shapes are efficient light absorbers with a large absorption cross section and can be used to improve laser ablation of cancer.^{4,5,6,7} For example, gold nano-shells with a silica core absorb light efficiently in the near infrared spectral region where human tissue has two transparency windows and can therefore be used to enhance the absorption of a laser beam and effectively destroy a tumor.^{3,8} Gold nanorods have also been extensively studied for use as efficient absorbers of infrared light in the near infrared spectral region.⁹ However, the penetration depth of infrared light in the body of a patient is limited and thus, only a limited number of cancers can be treated with this method, such as melanoma or prostate.

Electromagnetic waves in the radiofrequency (RF) domain can penetrate deep into the human body allowing for broader use of the hyperthermia treatment of cancer.⁴ RF hyperthermia mediated with gold nanoparticles as heat nanotransducers is a promising minimally invasive method for the targeted treatment of cancer.¹⁰ Gold nanoparticles have been recently shown to be effective heat nanotransducers under RF excitation at 13.56 MHz.^{4,11} The first demonstration of the heating of gold nanoparticles was introduced by John Kanzius in 2010.^{4,11} The RF system he designed is known as a “Kanzius Machine” and is used by many groups to study hyperthermia with gold nanoparticles.^{4,12,13,14}

Since the first publications on heat production by gold nanoparticles, the heating mechanism during exposure of colloidal gold to RF electromagnetic waves has been the subject of debate in the literature.^{15,16,17,18} Careful calculations of the Joule heat resulting from induced currents within the gold nanoparticles was shown to be insufficient to account for the temperature increase by the gold colloids under RF exposure.^{18,19,20} The contribution of the heat produced by the ionic background was later studied as a possible mechanism. Recently, the electrophoretic motion of the ions induced by the applied RF field was proven to be a major source of the heat produced by the gold colloidal solutions.^{16,21} The heat generated by the gold nanoparticles was then separated from the heat produced by the ionic buffer solution through the use of careful purification protocols designed for the gold colloids.²²

Although there have been a number of papers on the heating of gold nanoparticles, most of the experimental studies were conducted at the single frequency 13.56 MHz and for a limited number of nanoparticle sizes.¹⁸ Practical clinical application of RF hyperthermia requires flexibility in E-field frequency and nanoparticle size. Therefore, a systematic study of the heat generation of gold

nanoparticles of various sizes exposed to RF waves at various frequencies is highly desirable in order to facilitate the clinical translation of RF hyperthermia with gold nanoparticles.

Here we report an experimental study on the heat production and heating rates for gold nanoparticles of diameters 5, 10, 20, and 30 nm exposed to an RF E-field at frequencies 6.5, 8.2, 10, 13.56, 15, and 17 MHz each with a peak-to-peak potential maintained in the region of 950-980 V. The heating of gold nanoparticles was registered with an optical fiber inserted into a cuvette with gold colloid. A signal generator with an amplifier and impedance matching unit was used to deliver the RF waves to a capacitively coupled unit with the cuvette holder placed inside the capacitor. We used the energy balance equation to calculate the theoretical heating profile of gold colloid as a function of time.

Results and Discussion

Gold nanoparticles exhibit collective oscillations of free electrons known as Localized Surface Plasmon Resonance (SPR) when exposed to visible light as shown in Fig. 1.^{23,24,25} For all of the gold nanoparticle

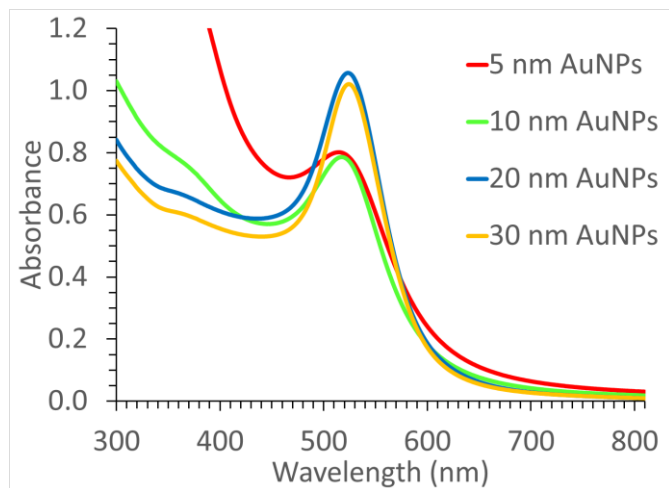


Figure 1. UV-visible extinction spectra of spherical gold nanoparticles in RF E-field heat generation experiments. The SPR peak in the extinction spectra is around 520 nm for all nanoparticles sizes used in this study.

sizes studied here, SPR occurred at nearly the same wavelength. The heating of the colloidal solutions under RF E-field does not lead to any noticeable change in the extinction spectra indicating that the nanoparticles are stable under heating from the room temperature up to $\sim 30^{\circ}\text{C}$. We note that the SPR does not play a substantial role in the heating of colloidal gold as the induced currents inside the nanoparticles have been calculated to be insufficient at explaining the temperature increase. Rather, the heating is primarily

the result of the electrophoretic motion of ions around the gold nanoparticles. However, the SPR provides information on the stability of the colloidal solution during the heating experiments.

Most of the studies on the RF heating of gold nanoparticles reported so far have used the RF frequency 13.56 MHz following the first report by Kanzius,⁴ with the frequency choice dictated primarily by the equipment available for the study. Here we report the heating profiles of gold nanoparticles of a few different diameters at several frequencies.

Fig. 2 below shows the experimental heating profiles of gold nanoparticles at the frequencies 10 MHz (a), 13.56 MHz (b), and 15 MHz (c). The change in temperature is measured relative to the ambient laboratory temperature as measured using the same fiber optic probe used in the experiment. The applied capacitively coupled RF E-field is turned on at the time $t = 0$ s and then the system is turned off at the time $t \approx 3200$ s once the temperature of the colloidal solution is plateaued indicating temperature equilibrium with the ambient atmosphere. The temperature data acquired prior to the system being turned on is used to determine the ambient laboratory temperature. The voltage across the capacitor was kept in the range of 950-980 V during all heating experiments. The voltage was verified with an oscilloscope at the beginning of the experiment.

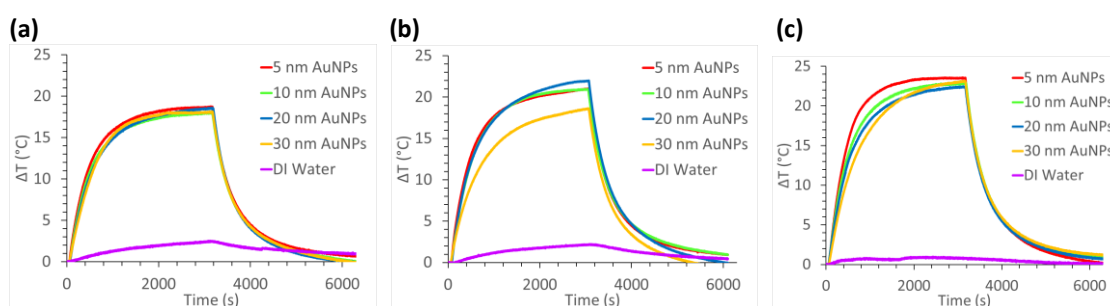


Figure 2. Heating profiles of gold nanoparticles of different sizes exposed to RF E-fields in the range of 950-980 V. The E-field is turned on initially and is turned off after the temperature saturates at the equilibrium temperatures defined by the plateau. The frequency of the applied RF E-field is: (a) 10 MHz, (b) 13.56 MHz, (c) 15 MHz. The heating profiles are shown for 5, 10, 20, and 30 nm gold nanoparticles as well as for DI water.

The plots reveal that the heating due to RF exposure is significantly higher for gold colloids than for deionized (DI) water. The equilibrium (plateau) temperature shows some frequency dependence with nanoparticles of all sizes plateauing at ~ 18 °C when exposed to 10 MHz RF waves and plateauing at ~ 23 °C when exposed to 15 MHz RF waves. At each of the frequencies shown, the heating curve of DI water did not exceed 3 °C. Heating curves at 13.56 MHz were obtained in quadruplicate for each size and are consistent with previously published results. The heating of gold nanoparticles at the frequency 10 MHz is similar but with generally lower heating rates.

In Fig. 3 below, the same heating and cooling curves of colloidal gold suspensions are presented for all frequencies but are grouped according to nanoparticle diameter. Here it is even more apparent that an increase in the frequency leads, in general, to a higher saturation temperature. The highest saturation equilibrium temperature observed was ~ 28 °C for 10 nm gold nanoparticles exposed to RF waves at 17 MHz (Fig. 3 (b)). For all other sizes of gold nanoparticles (AuNPs), the highest saturation

temperature observed occurred at 15 MHz and was ~ 23.5 °C for 5 nm AuNPs, ~ 22.4 °C for 20 nm AuNPs, and ~ 23 °C for 30 nm AuNPs. The 5 and 10 nm AuNPs were exposed to frequencies as high as 17 MHz, while the 20 and 30 nm AuNPs were exposed to frequencies as high as 15 MHz.

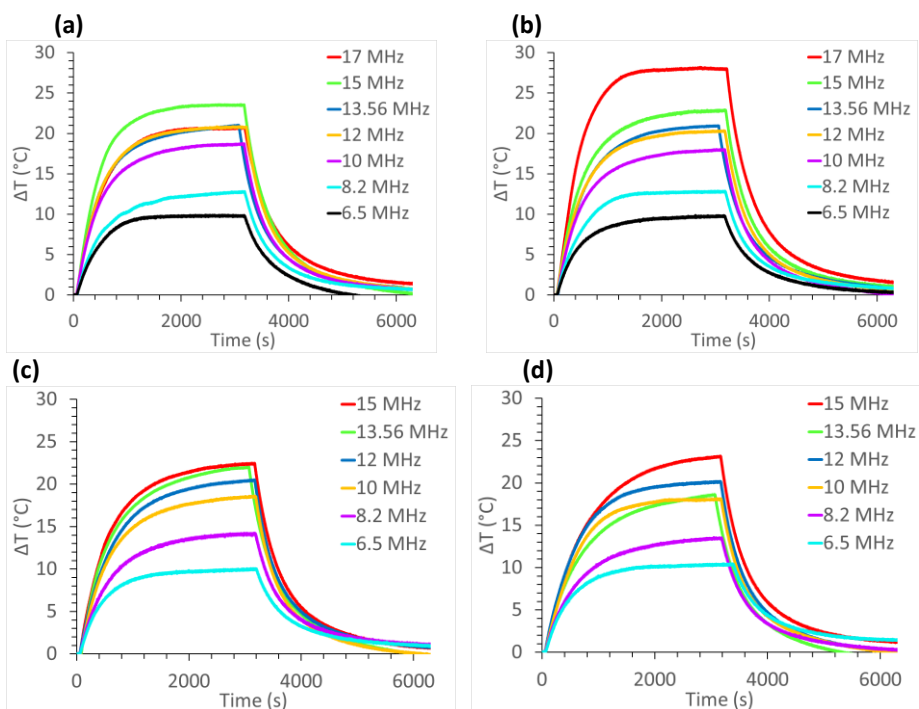


Figure 3. Heating profiles of gold nanoparticles of different sizes exposed to RF E-fields in the range of 950-980 V. (a) 5 nm gold nanoparticles. (b) 10 nm gold nanoparticles, (c) 20 nm gold nanoparticles, (d) 30 nm gold nanoparticles. The E-field is turned on initially and is turned off after the temperature saturates at the equilibrium temperatures defined by the plateau.

The heating rate (initial slope of the heating curve) of gold colloids depends on the size of the gold nanoparticles and the frequency of the RF field as shown in Fig. 4. The heating rate was interpolated for each experiment by applying a linear fit to 50 of the first several hundred data points in the heating curves. Interpolation of the heating rates observed at varying frequencies reveals that the maximum heating rate for 5, 10 and 20 nm AuNPs is observed at 13.56 MHz, see Fig. 4 (a, b and c). However, 30 nm AuNPs exhibit a maximum heating rate at 12 MHz, Fig. 4 (d).

A polynomial fit of the data reveals a maximum heating rate for the 5 and 30 nm gold colloids near 14 and 13 MHz respectively. The maximum heating rate for the 10 nm gold colloid as determined from the polynomial fit falls above 17 MHz. 17 MHz was the highest frequency with which both the 5 and 10 nm colloids were RF heated while 15 MHz was the highest frequency used to heat the 20 and 30 nm colloids. The polynomial fit of the 20 nm data does not show a maximum rate in the 6.5 to 17 MHz range

and is quite linear. These patterns deserve further theoretical investigations to explain the size and frequency dependence of the experimentally observed heating rates.

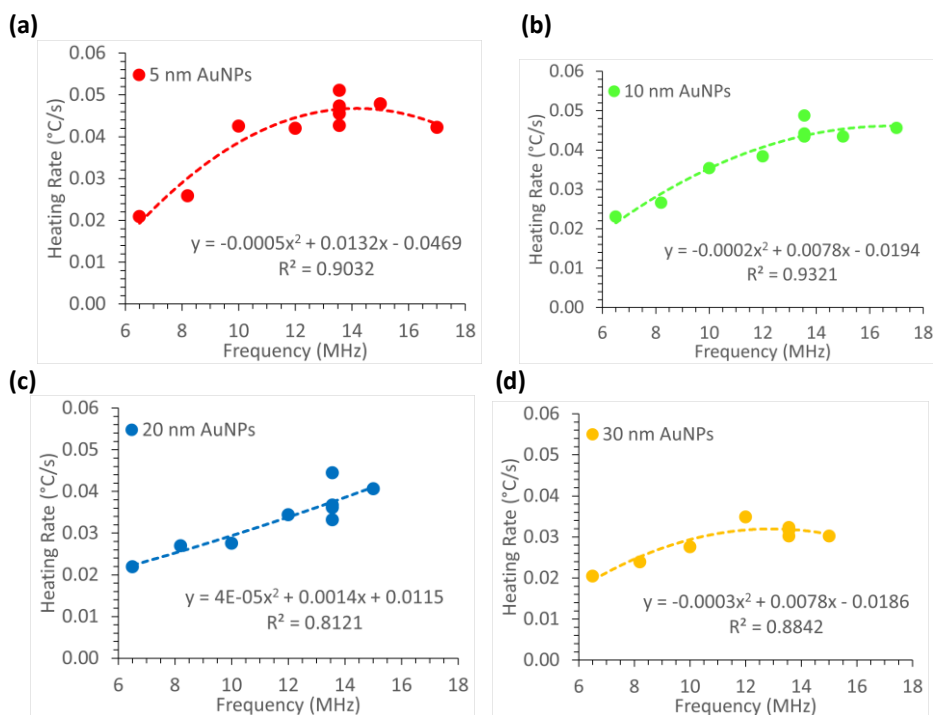


Figure 4. Heating rates of gold colloidal solutions as a function of the applied RF E-field frequency for 5 nm (a), 10 nm (b), 20 nm (c), and 30 nm gold nanoparticles (d).

Concentration dependent measurements were also performed and show that heating is dependent on the mass of gold present in the solution. As the concentration decreases, the rise in temperature also decreases, as shown in Fig. 5. Each stock solution was diluted by a factor of 2.5, 5, and 10 with ultrapure water (UPH₂O, 18.1 MΩ resistivity) to understand the dependence on the mass of gold on heating. As expected, the subsequent dilutions of the 5 nm AuNPs heated more significantly than those of the 20 and 30 nm AuNP solutions. Ultrapure water (UPH₂O) was used to dilute the stock solutions and background heating from water was subtracted from all diluted samples.

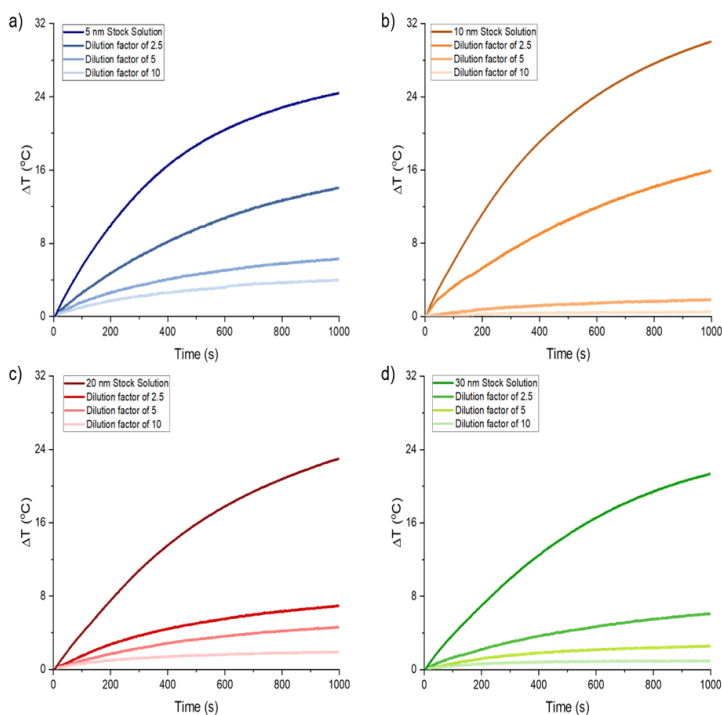


Figure 5. Temperature change for different concentrations of a) 5 nm, b) 10 nm, c) 20 nm and d) 30 nm gold nanoparticles.

We want to emphasize that the goal of this paper is not to specifically examine the heat produced by the gold nanoparticles versus the heat produced by the ionic buffer. Rather, the aim was to study the effects of nanoparticle size and RF field frequency on heat generation. However, to prove that the heat generated by aqueous colloidal gold can be separated into heat produced by the gold nanoparticles and heat produced by the buffer, we centrifuged the colloids to demonstrate the contribution to the heat produced by the ionic background without the gold nanoparticles. When comparing the heating of the gold colloid to the supernatant of those solutions, we found the presence of gold contributed to a 42% increase in overall heating as shown in Fig. 6. The supernatants were centrifuged a total of three times and the temperature was measured after each subsequent centrifugation. Fig. 6 shows that the resulting supernatants heat much less and at a slower rate than their stock solution counterparts. Furthermore, gold nanoparticles of size 20 nm suspended in DI water were also purchased from another vendor (Nanopartz, Colorado) and further confirmed the heat generated by the gold nanoparticles, see Fig. S2.

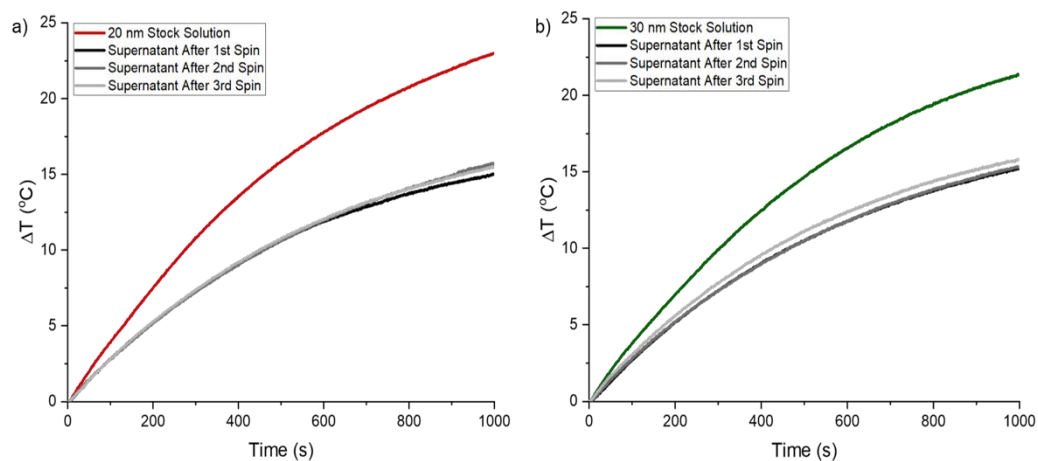


Figure 6. Stock solution and supernatant heating of a) 20 nm AuNPs and b) 30 nm AuNPs. The supernatant heats about 7 and 5.5 °C less than the corresponding stock solution of the 20 nm and 30 nm AuNPs, respectively. The authors would like to note here that the size of the 5 nm AuNPs make it especially challenging to remove the particles and the yellow color of the resulting supernatant indicates that gold particles or atoms remained.

Fig. 7 (a) shows the experimental and theoretical heating profiles of gold colloids of size 20 nm. The theoretical calculations were carried out by using the energy balance equations as outlined in the next section. The dissipation constant B was obtained by fitting the cooling portion of the heating experiment as shown in Fig. 7 (b). Comparison of the experimental and theoretical temperature profiles was done for 13.56 MHz RF waves. For the theoretical calculation, it was assumed that $Q_{in} = 0.54 J$. The experimental data show in Fig. 7 (a) was obtained using nanoparticles purchased from Nanopartz (Colorado, USA). All other experimental curves plateaued below the one shown above. Excellent agreement is seen between the theoretical numerical calculations and the experimental results.

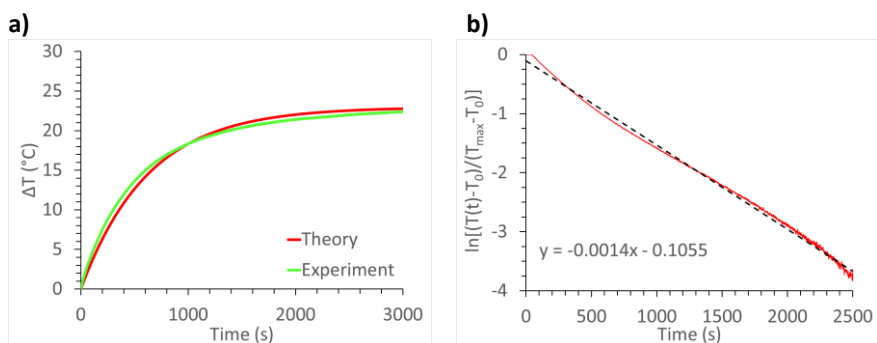


Figure 7. Comparison of the experimental and theoretical temperature profiles of 20 nm gold colloids heated at a frequency of 13.56 MHz (a). Determination of the dissipation constant B by a linear fit of the first 2500 s of the cooling curve (b).

Conclusion

Nanoparticles of various materials, sizes, and morphologies continue to be of interest for cancer therapy based on hyperthermia. The current technologies, including chemotherapy and ablation, are uncomfortable for the patient as well as costly and new technologies are needed to alleviate costs and effectively treat patients with minimal side effects. Gold nanoparticles are ideal for these types of applications because they are cost-effective and are relatively easy to make and surface-modify.

Using electromagnetic waves to heat metal nanoparticles is promising as a treatment for metastatic cancers since metal particles have the potential to heat in both electric fields and magnetic fields. Radiofrequencies, in particular, are an ideal candidate for this as they penetrate through non-conductive materials like human tissue. Gold nanoparticles exposed to a capacitively coupled electric field in the MHz frequency range generate heat that might be used in the hyperthermia treatment of cancer. Here we experimentally demonstrated RF-induced heat generated by spherical gold nanoparticle colloids in the size range of 5 nm to 30 nm that is sufficient for hyperthermia applications. We also show experimentally that gold nanoparticle colloids exhibit significant heating rates in the frequency range 6.5 MHz to 17 MHz. Finally, using the energy balance equations we demonstrated that the experimental heating profiles can be modeled numerically with the calculated dissipation rate B . This work demonstrates that the heating of gold solutions is not necessarily limited by size or frequency but depends more on the concentration of gold and the electric field applied. The results of the study may be helpful in the development of safe, non-invasive efficient hyperthermia treatments for various cancers including metastatic cancers.

Experimental and Theoretical Methods

Materials and equipment. Gold nanoparticles of various sizes were purchased from Ted Pella (Redding, CA). Each size of nanoparticle (5, 10, 20, and 30 nm) was citrate capped and suspended in a buffer solution maintaining the colloidal suspension. A Hewlett Packard 9 kHz-3200 MHz signal generator (8648C) was purchased from Liberty Test Equipment (Roseville, CA) and used to provide the RF signal to the rest of the setup. An AR 10 kHz-250 MHz, 125 W continuous wave power amplifier (125A260M6) was purchased from TMS Sales (Greenwood Village, CO) to amplify the signal from the signal generator. An MFJ rolling inductor antenna tuner (MFJ-989D) was purchased from R & L Electronics (Hamilton, OH) and used to tune the RF input to provide impedance matching to the system. All cables and connections used in the setup were purchased from Pasternack (Irvine, CA). The fiber optic temperature sensor and conditioning box (TempSens) were purchased from OpSens (Quebec City, Quebec, Canada) and were used with the OpSens SoftSens software to collect data. The capacitor was designed and built in-house with materials purchased from local hardware stores.

The capacitor was designed to achieve a high electric field across the plates, so space between the plates was minimized. The plates of the capacitor are made from copper sheets and measure 25 cm x 25 cm. They are fixed to plexiglass to make the plates easier to move when changing samples. A schematic of the capacitor and overall set up is shown in Fig. 8. Pictures of the setup can be seen in Figs. S3 and S4 in the supporting information.

For each experiment, 3.5 mL of the solution of interest was placed into a standard plastic cuvette. A cap with a hole punched through the top—large enough for the fiber optic temperature sensor—was used to prevent evaporation as well as hold the sensor in place during measurements. The signal generator was set to 190.001 mV emf and the gain on the power amplifier was adjusted to either maximize the voltage across the plates (in the case of the temperature profiles, supernatant comparisons, and concentration dependence experiments) or to adjust the power in the case of the power dependence experiments. The tuning box was used as a resonance circuit and the capacitance and inductance were tuned accordingly. A Keysight InfiniiVision oscilloscope (DSO-x-2014A, Keysight Technologies, Santa Rosa, CA) was used to measure the voltage across the plates at the beginning to each experiment. Voltage measurements were obtained using a 100:1 probe. For the gain/power dependent measurements, the voltage was recorded for each solution at predetermined gain percentages.

For the concentration dependent experiments, the stock solutions of the 5, 20, and 30 nm solutions were diluted by a factor of 2.5, 5, or 10 using ultrapure water (UPH₂O) with a measured resistivity of 18.1 M Ω . 3.5

mL of the corresponding diluted sample was placed into a standard plastic cuvette and measured as described above.

For the supernatant experiments, the 20 and 30 nm particles were spun in a Spectrafuge 16M Brushless Laboratory Microcentrifuge at 10,000 and 6,000 rpm, respectively, for 30 minutes. The supernatant was then collected, measured, and spun again. This was repeated for a total of three times to ensure thorough washing of the particles and to remove any residual gold in the supernatant. The 5 nm particles require higher centrifuge speeds and were spun in a Thermo Sorvall MX120+ ultracentrifuge at 100,000 rcf for 30 minutes.

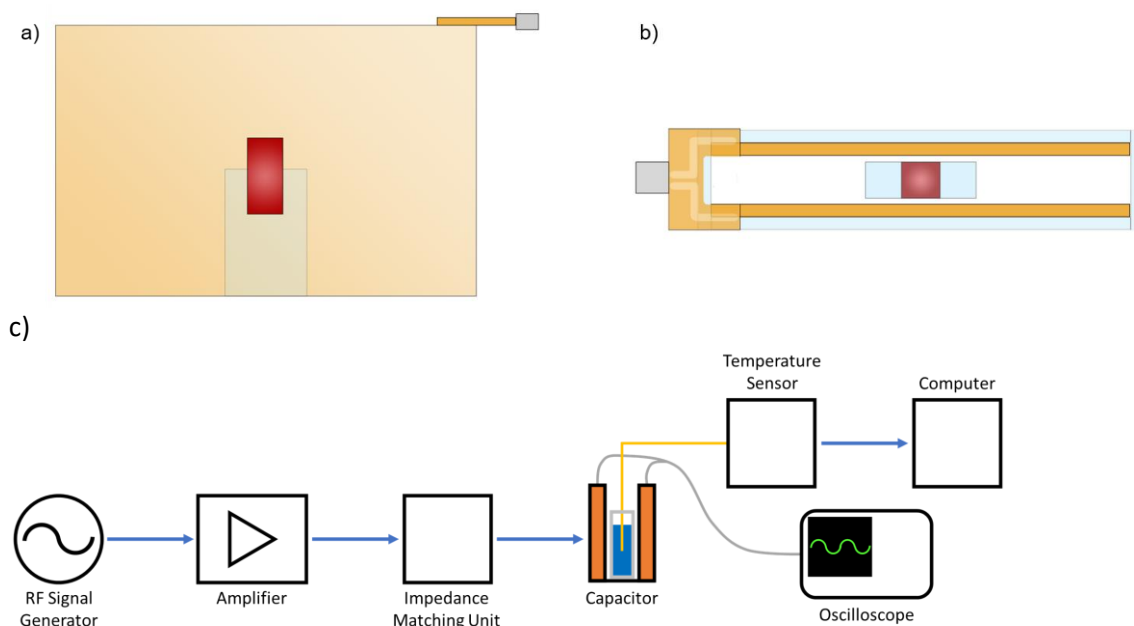


Figure 8. a) Side view and b) top view of the parallel plate capacitor set up. The red rectangle indicates the gold nanoparticle solution contained within a plastic cuvette. This cuvette is placed within a plastic stand that is fixed between the two plates to minimize samples movement between measurements. A BNC connection is soldered to a PCB which is connected to the copper plates to deliver the signal. (c) Schematic diagram of the heating experimental setup. The RF E-field in the capacitor was produced by an RF signal generator connected to an amplifier and an impedance matching unit. The two plates of the capacitor were attached to an oscilloscope to verify frequency and measure peak-to-peak potential. A temperature probe placed in the sample was connected to a temperature sensor monitored by a computer.

Theory. The change in thermal energy of gold colloidal solution exposed to an external electromagnetic field satisfies the energy balance equation ^{5,23}

$$\sum_i m_i C_i \frac{dT}{dt} = Q_{in} - Q_{out} , \quad (1)$$

where m_i and C_i are the mass and specific heat capacity of the solution, T is the temperature of the solution, and t is time during which the input heat from RF power (Q_{in}) is absorbed by the gold nanoparticles and the output heat (Q_{out}) is dissipated to the environment. The mass and specific heat capacity of gold colloids are much smaller than that of water. Hence Eq. (1) can be simplified as

$$m_W C_W \frac{dT}{dt} = Q_{in} - Q_{out} , \quad (2)$$

where m_i and C_i are the mass and specific heat capacity of the water, respectively.

The input heat that is absorbed by gold nanoparticles is given as

$$Q_{in} = (I_0 - I_{tr})\eta, \quad (3)$$

where I_0 is the incident power, I_{tr} is the power transmitted through the solution, and η is the RF conversion efficiency.

The heat dissipated by the system is given as

$$Q_{out} = hS(T(t) - T_0) , \quad (4)$$

where h is the heat transfer efficiency, S is the surface area of the cuvette, $T(t)$ is the temperature at time t , and T_0 is the room temperature.

Using Eq. (3)-(4), Eq. (2) can be rewritten as

$$\frac{d\Delta T}{dt} = \frac{(I_0 - I_{tr})}{m_W C_W} \eta - B\Delta T , \quad (5)$$

We define $\Delta T = T(t) - T_0$ as the change in temperature and $B = \frac{hS}{m_W C_W}$ as the constant rate of heat dissipation from the gold nanoparticles to the environment. B can be determined by tracing the

temperature decay back to the ambient temperature after the RF field is turned off. In this regime the temperature trace is given by

$$T(t) = T_0 + (T_{max} - T_0)\exp(-Bt) , \quad (6)$$

where T_{max} is the maximum temperature when RF power is off.

At the thermal equilibrium (Q_{in} equals to Q_{out}), the temperature is constant. Therefore, by setting Eq. (5) equal to zero, we can get

$$\Delta T = \frac{(I_0 - I_{tr})}{m_W c_W B} \eta . \quad (7)$$

Finally, using limit $T(0) = T_0$ and the expression for ΔT (Eq. (7)), we can solve the differential equation (Eq. (5)) for $T(t)$ when the RF power is turned on

$$T(t) = T_0 + \frac{(I_0 - I_{tr})}{m_W c_W B} \eta (1 - \exp(-Bt)) \quad (8)$$

Acknowledgements

This publication is based on work supported by a grant from the U.S. Civilian Research & Development Foundation (CRDF Global). Any opinions, findings and conclusions or recommendations expressed in this material are those of the author(s) and do not necessarily reflect the views of CRDF Global. M.A. acknowledges support from Taibah University. We thank Kristen Petersen for administrative assistance.

Funding

This work was funded by the UCCS BioFrontiers Center and by CRDF Global, Project 65495.

References.

1. Sung, H.; Ferlay, J.; Siegel, R. L.; Laversanne, M.; Soerjomataram, I.; Jemal, A.; Bray, F. Global cancer statistics 2020: GLOBOCAN estimates of incidence and mortality worldwide for 36 cancers in 185 countries. *CA: A Cancer Journal for Clinicians* **2021**, *71*, 209-249.
2. Mayo Clinic Staff. Cancer survivors: Late effects of cancer treatment. Mayo Clinic <https://www.mayoclinic.org/diseases-conditions/cancer/in-depth/cancer-survivor/art-20045524> (2020).
3. Hirsch, L. R.; Stafford, R. J.; Bankson, J. A.; Sershen, S. R.; Rivera, B.; Price, R. E.; Hazle, J. D.; Halas, N. J.; West, J. L. Nanoshell-mediated near-infrared thermal therapy of tumors under magnetic resonance guidance. *Proceedings of the National Academy of Sciences* **2003**, *100*, 13549-13554.
4. Abadeer, N. S.; Murphy, C. J. Recent progress in cancer thermal therapy using gold nanoparticles. *Nanomaterials and Neoplasms* **2021**, 143-217.
5. Alrahili, M.; Peroor, R.; Savchuk, V.; McNear, K.; Pinchuk, A. Morphology dependence in photothermal heating of gold nanomaterials with near-infrared laser. *The Journal of Physical Chemistry C* **2020**, *124*, 4755-4763.
6. Jiang, K.; Smith, D. A.; Pinchuk, A. Size-dependent photothermal conversion efficiencies of plasmonically heated gold nanoparticles. *The Journal of Physical Chemistry C* **2013**, *117*, 27073-27080.
7. Anselmo, A. C.; Mitragotri, S. Nanoparticles in the clinic: An update. *Bioengineering & translational medicine* **2019**, *4*, e10143.
8. Rastinehad, A. R.; Anastos, H.; Wajswol, E.; Winoker, J. S.; Sfakianos, J. P.; Doppalapudi, S. K.; Carrick, M. R.; Knauer, C. J.; Taouli, B.; Lewis, S. C. Gold nanoshell-localized photothermal ablation of prostate tumors in a clinical pilot device study. *Proceedings of the National Academy of Sciences* **2019**, *116*, 18590-18596.
9. Huang, X.; El-Sayed, I. H.; El-Sayed, M. A. In *Applications of gold nanorods for cancer imaging and photothermal therapy*; Cancer nanotechnology; Springer: 2010; pp 343-357.
10. Corr, S. J.; Raoof, M.; Mackeyev, Y.; Phounsavath, S.; Cheney, M. A.; Cisneros, B. T.; Shur, M.; Gozin, M.; McNally, P. J.; Wilson, L. J.; Curley, S. A. Citrate-Capped Gold Nanoparticle Electrophoretic Heat Production in Response to a Time-Varying Radio-Frequency Electric Field. *Journal of Physical Chemistry C* **2012**, *116*, 24380-24389.
11. Corr, S. J.; Curley, S. A. In *Gold nanoparticles for noninvasive radiofrequency cancer hyperthermia*; Nanotechnology in Cancer; Elsevier: 2017; pp 1-18.
12. Raoof, M.; Corr, S. J.; Zhu, C.; Cisneros, B. T.; Kaluarachchi, W. D.; Phounsavath, S.; Wilson, L. J.; Curley, S. A. Gold nanoparticles and radiofrequency in experimental models for hepatocellular carcinoma. *Nanomedicine: Nanotechnology, Biology and Medicine* **2014**, *10*, 1121-1130.

13. Glazer, E. S.; Zhu, C.; Massey, K. L.; Thompson, C. S.; Kaluarachchi, W. D.; Hamir, A. N.; Curley, S. A. Noninvasive radiofrequency field destruction of pancreatic adenocarcinoma xenografts treated with targeted gold nanoparticles. *Clinical Cancer Research* **2010a**, *16*, 5712-5721.
14. Chen, C.; Chen, C.; Li, J.; Chen, Y.; Wang, C.; Wang, Y.; Chi, K.; Wang, H. Presence of Gold Nanoparticles in Cells Associated with the Cell-Killing Effect of Modulated Electro-Hyperthermia. *ACS Applied Bio Materials* **2019**, *2*, 3573-3581.
15. Li, D.; Jung, Y. S.; Tan, S.; Kim, H. K.; Chory, E.; Geller, D. A. Negligible absorption of radiofrequency radiation by colloidal gold nanoparticles. *J. Colloid Interface Sci.* **2011**, *358*, 47-53.
16. Collins, C. B.; Tofanelli, M. A.; Noblitt, S. D.; Ackerson, C. J. Electrophoretic mechanism of Au₂₅(SR)₁₈ heating in radiofrequency fields. *The journal of physical chemistry letters* **2018a**, *9*, 1516-1521.
17. Glazer, E. S.; Zhu, C.; Massey, K. L.; Thompson, C. S.; Kaluarachchi, W. D.; Hamir, A. N.; Curley, S. A. Noninvasive radiofrequency field destruction of pancreatic adenocarcinoma xenografts treated with targeted gold nanoparticles. *Clinical Cancer Research* **2010b**, *16*, 5712-5721.
18. Collins, C. B.; McCoy, R. S.; Ackerson, B. J.; Collins, G. J.; Ackerson, C. J. Radiofrequency heating pathways for gold nanoparticles. *Nanoscale* **2014**, *6*, 8459-8472.
19. Sassaroli, E.; Li, K.; O'Neill, B. E. Radio frequency absorption in gold nanoparticle suspensions: a phenomenological study. *J. Phys. D* **2012**, *45*, 075303.
20. Hanson, G. W.; Patch, S. K. Optimum electromagnetic heating of nanoparticle thermal contrast agents at rf frequencies. *J. Appl. Phys.* **2009**, *106*, 054309.
21. Collins, C. B.; Tofanelli, M. A.; Noblitt, S. D.; Ackerson, C. J. Electrophoretic mechanism of Au₂₅(SR)₁₈ heating in radiofrequency fields. *The journal of physical chemistry letters* **2018b**, *9*, 1516-1521.
22. Cherukuri, P.; Glazer, E. S.; Curley, S. A. Targeted hyperthermia using metal nanoparticles. *Adv. Drug Deliv. Rev.* **2010**, *62*, 339-345.
23. Alrahili, M.; Savchuk, V.; McNear, K.; Pinchuk, A. Absorption cross section of gold nanoparticles based on NIR laser heating and thermodynamic calculations. *Scientific reports* **2020**, *10*, 1-9.
24. Wei, Y.; Klajn, R.; Pinchuk, A. O.; Grzybowski, B. A. Synthesis, shape control, and optical properties of hybrid Au/Fe₃O₄ "Nanoflowers". *Small* **2008**, *4*, 1635-9.
25. Yeshchenko, O. A.; Dmitruk, I. M.; Alexeenko, A. A.; Losytskyy, M. Y.; Kotko, A. V.; Pinchuk, A. O. Size-dependent surface-plasmon-enhanced photoluminescence from silver nanoparticles embedded in silica. *Physical Review B (Condensed Matter and Materials Physics)* **2009**, *79*, 235438 (8 pp.).